Magnetic anisotropy of $R_2Fe_{14}B$ (R=Nd, Gd, Y): Density functional calculation by using the linear combination of pseudo-atomic-orbital method

Isao Kitagawa* and Yusuke Asari
Advanced Research Laboratory, Hitachi, Ltd., Kokubunji, Tokyo 185-8601, Japan
(Received 2 December 2009; revised manuscript received 15 April 2010; published 8 June 2010)

The magnetocrystalline anisotropy energy (MAE) of rare-earth transition-metal intermetallics $R_2Fe_{14}B$ (R=Nd, Gd, Y) was calculated by using the linear combination of pseudo-atomic-orbital method. Electronic structures were calculated by using relativistic density functional theory with Hubbard-type on-site Coulomb potential U for f electrons in the R sites. The calculated magnetic moments of $Y_2Fe_{14}B$ and $Gd_2Fe_{14}B$ are in agreement with the experimentally measured saturation moments of these compounds. The calculated MAEs of $Y_2Fe_{14}B$ and $Gd_2Fe_{14}B$ are also in agreement with the value measured at low temperature. Moreover, it was found that the shape of the charge density at the Nd sites is aspherical, which causes larger MAE of $Nd_2Fe_{14}B$ than that of $Gd_2Fe_{14}B$. However, the orbital moment of the 4f electrons at the Nd sites and the MAE of $Nd_2Fe_{14}B$ were underestimated within the scope of a relativistic local-density approximation plus U with spherical average potential.

DOI: 10.1103/PhysRevB.81.214408 PACS number(s): 71.20.Eh, 71.15.Mb, 71.15.Ap, 71.15.Rf

I. INTRODUCTION

Since the discovery of $Nd_2Fe_{14}B$ in 1984, neodymium-iron-boron (Nd-Fe-B) magnets have been developed for applications in a wide range of fields, such as magnetic-resonance imaging, electric vehicles, and hard-disk drives. $Nd_2Fe_{14}B$ and related materials have been actively studied because magnets based on $Nd_2Fe_{14}B$ not only is lower cost than magnets based on other rare-earth (R) transition-metal intermetallics, such as $SmCo_5$ but also have higher-energy product.[1] Recently, to increase the coercive force of the Nd-Fe-B-based magnet, dysprosium addition to the magnet has been introduced; however, the mechanism that enhances the coercive force is still unclear. In research on such a high-coercivity magnet, understanding the origin of the magnetocrystalline anisotropy energy (MAE) which is based on electronic structure is a key issue.

MAE is the change in total energy of a ferromagnet when the magnetic moment is rotated through angles θ and ϕ, where θ and ϕ are the polar and azimuth angles, respectively. There are two methods for estimating MAE. One is the crystal electric field (CEF) calculation, which is based on charge distribution obtained from band-energy calculations and is of great importance in explaining the magnetic anisotropy of R transition-metal compounds.[2–5] To estimate MAE, the energy that is expressed by means of interaction between localized 4f electron and the CEF is calculated by using Stevens' operators.[6] The value of radial density of the 4f electrons influences to the energy of the interaction between the 4f electron and the CEF. Thus, correct treatment for the 4f electrons such as fully relativistic calculation is needed for the CEF calculation. Moreover, it is difficult to estimate the contribution of a transition metal to MAE by means of this method.

The other method is to directly calculate the change in total energy with respect to the direction of the magnetic moment. If the electronic structure of the R transition-metal intermetallics is correctly treated, the contributions of both the R and transition-metal atoms to MAE can be estimated. This approach was first applied to the 3d transition-metal bulk and thin film in which spin-orbit coupling interaction (SOI) makes the main contribution to MAE.[7–10] Recently, the calculation of MAE of hcp gadolinium (Gd) in fully relativistic density functional theory (DFT) within the local-spin-density approximation (LSDA) was reported.[11] In this paper, it is shown that the dipole-dipole interaction between the large localized 4f spins and the SOI of the band electrons are two major contributions to MAE. However, it has not yet been attempted to calculate the electronic structure of an intricate system such as $R_2Fe_{14}B$ type intermetallics that contain the open shell of the 4f electrons.

The nonself-consistent electronic structure of $R_2Fe_{14}B$ compounds were calculated by Gu and Ching using orthogonalized linear combination of atomic orbitals (OLCAO) method.[12,13] The first self-consistent electronic structure of $Nd_2Fe_{14}B$ by using linear-muffin-tin-orbital method was reported by Jaswal,[14] whether the 4f states of neodymium was ignored or incorporated as a core. The localized 4f spin magnetization density was incorporated in the electronic-structure calculation within nonrelativistic LSDA by Nordström *et al.*[15] However, it has not yet been attempted to calculate the electronic structure of an intricate system such as $R_2Fe_{14}B$-type intermetallics that contain the open shell of the 4f electrons with fully relativistic treatment.

In regard to large-scale and complex systems, it is important to reduce the complexity of the electronic-structure calculation while maintaining calculation accuracy. Recently, a first-principles calculation using the linear combination of pseudo-atomic-orbital (LCPAO) method has been developed and applied to reveal the physical mechanism of various materials.[16–20] The variationally optimized numerical atomic-orbital basis set, which is called PAO is constructed by using a norm-conserving pseudopotential. The LCPAO method makes it possible to reduce the size of the Hamiltonian matrix and perform noncollinear calculation with fully relativistic treatment. The LCPAO method thus has the potential to calculate MAE of large-scale systems but the accuracy is unknown for the R transition-metal intermetallics.

TABLE I. Lattice constants, MAE, and total magnetic moment (M_s) of $R_2Fe_{14}B$ (R=Nd, Gd, Y) compounds.

	Lattice (nm)		MAE (MJ/m^3)		M_s (μ_B/f.u.)	
Compounds	a	c	Calc.	Expt.	Calc.	Expt.
$Y_2Fe_{14}B$	0.876	1.200	0.56	0.75[a]	32.85	31.4[a]
$Gd_2Fe_{14}B$	0.874	1.194	0.67	0.58[a]	18.60	17.9[a]
$Nd_2Fe_{14}B$ (ferro)	0.880	1.219	2.24	4.27[b]	41.61	42.84[a]
$Nd_2Fe_{14}B$ (ferri)	0.880	1.219	1.35	4.27[b]	26.86	42.84[a]

[a]Reference 27 with 4.2 K.
[b]Reference 27 with room temperature.

In this study, we performed relativistic DFT calculation by using the LCPAO method with Hubbard-type on-site Coulomb potential U for the f electrons at the R sites. We show that the calculated magnetic moments of $Y_2Fe_{14}B$ and $Gd_2Fe_{14}B$ are in agreement with the measured ones. Moreover, the calculated MAEs of $Y_2Fe_{14}B$ and $Gd_2Fe_{14}B$ are also in agreement with the MAEs measured at low temperature. We also found that the charge-density distribution at the Nd sites has an aspherical shape that causes the MAE of $Nd_2Fe_{14}B$ to be larger than that of $Gd_2Fe_{14}B$. In Sec. II, we discuss the details of calculation of the electronic structure of $R_2Fe_{14}B$ system. The calculated electronic structures of these three compounds are presented in Sec. III A. Then, the calculated MAE value and the convergency of the MAE are discussed in Sec. III B. In Sec. III C, we discuss the magnetic moments and charge distribution. Finally, the efficacy of the LCPAO method is discussed in Sec. IV.

II. COMPUTATIONAL DETAILS

The symmetry of an electronic structure with a magnetic moment is characterized by a transformation that involves a reversal of moment direction. The symmetry with magnetization is lower than the space group of a crystal. For the MAE calculation, the electronic structure thus has to be calculated under low symmetry. MAE was evaluated as the difference between the total energy when magnetization is parallel to the c axis and that when it is parallel to the a axis. A tetragonal unit cell with space group P_1 (which has 68 atoms) was used for the MAE calculation. Since the total-energy difference strongly depends on the number of k points in the mesh in the first Brillouin zone, a mesh with $4\times4\times4$ (64) k points was used in a self-consistent calculation and up to 2744 k points were used in the MAE calculation.

The open-source OPENMX program was used to perform self-consistent first-principles electronic-structure calculations.[16–19,21] OPENMX solves the Kohn-Sham equations of DFT by using a PAO basis set and norm-conserving pseudopotentials. The generalized gradient approximation proposed by Perdew *et al.* was used to describe electronic exchange and correlation.[22]

For ordinary LSDA calculation of R transition-metal intermetallics, by letting the $4f$ states form very narrow band near the Fermi energy, there will be serious numerical problem. Since the shallow $4f$ band is caused by lack of on-site Coulomb interaction on the f electron, the Hubbard-type on-site Coulomb potential U acting on the f electron was added to the DFT Hamiltonian and self-consistent calculations were performed.[19] According to Dudarev *et al.*, we used spherical averaged potential U within rotationally invariant functional formation for local-density approximation (LDA) plus U.[23] The value of U, 6.0 eV, for the Nd sites was determined in order to reproduce the magnetic moment $6.0\mu_B$ and the experimental lattice constant, a=3.831 Å of sesquioxide Nd_2O_3.[24] Literature value of the reference, 5.8 eV was used for the Gd site.[25]

$R_2Fe_{14}B$ crystal is a tetragonal unit cell with a space group of $P4_2/mnm$.[26] The unit cell has two different R sites, i.e., f and g, six distinct Fe sites (labeled $j1$, $j2$, $k1$, $k2$, e, and c), and one B site for a total of 68 atoms. Table I lists the measured lattice constants of $Y_2Fe_{14}B$, $Gd_2Fe_{14}B$, and $Nd_2Fe_{14}B$ used in this work.[27]

Two magnetic configurations of $4f$ and $3d$ spin sublattice are considered for $Nd_2Fe_{14}B$. One is ferromagnetic configuration between $4f$ and $3d$ spin sublattice. The other is ferrimagnetic configuration between $4f$ and $4d$ spin sublattice.

III. RESULTS

A. Electronic structure

Spin-resolved density of states (DOS) of $Y_2Fe_{14}B$, $Gd_2Fe_{14}B$, and $Nd_2Fe_{14}B$ are shown in Fig. 1. In $Y_2Fe_{14}B$, there are high-intensity DOS in the range from −5.0 to 0.0 eV of the majority-spin band and that in the range from −5.0 eV to 7.0 eV of the minority-spin band [see Fig. 1(a)]. These high-intensity DOS are mainly composed of $3d$ states of the Fe sites. Since the $3d$ states of Fe sites of the majority spin are only located below Fermi energy, the $3d$ spin moment exists on each Fe site. In $Gd_2Fe_{14}B$, there are narrow and high-intensity peaks of $4f$ electrons at −12.0 eV of the majority-spin band and that at 8.0 eV of the minority-spin band [see Fig. 1(b)]. In $Nd_2Fe_{14}B$, there are the narrow and high-intensity peaks of $4f$ electrons at −2.0 eV and 7.0 eV of the majority-spin band and that at 13.0 eV of the minority-spin band [see Fig. 1(c)]. The $3d$ states on the Fe sites of $Gd_2Fe_{14}B$ and $Nd_2Fe_{14}B$ have similar distribution of that of $Y_2Fe_{14}B$.

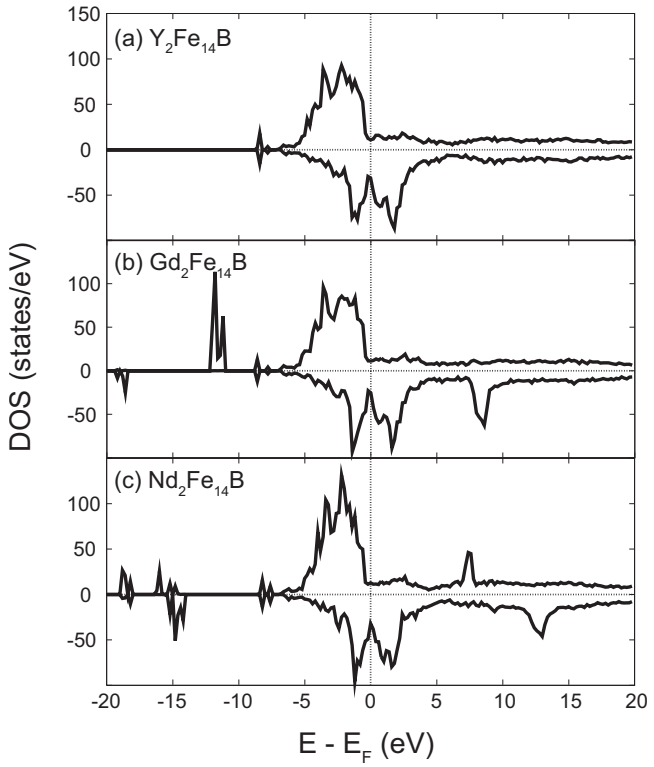

FIG. 1. Spin-resolved density of states of $Y_2Fe_{14}B$, $Gd_2Fe_{14}B$, and $Nd_2Fe_{14}B$. The directions of the spin moments are parallel to c axis. The majority (minority) spin states are above (below) the zero axis.

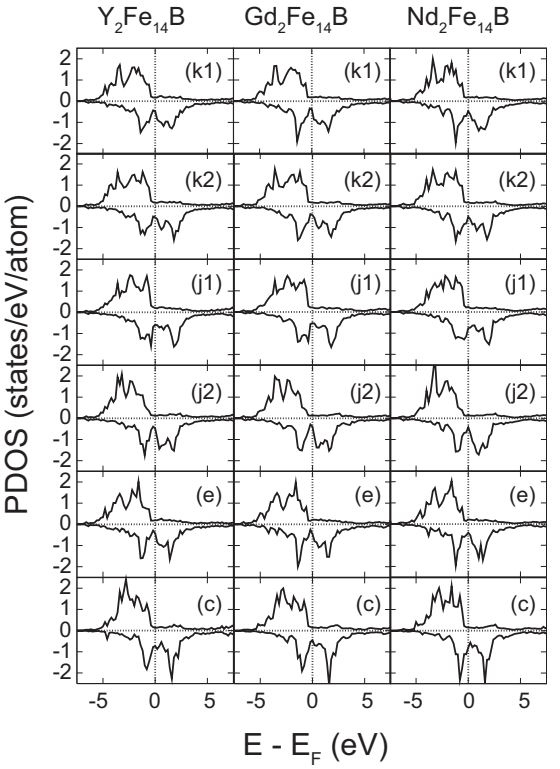

FIG. 2. Spin-resolved density of states on the Fe sites of $Y_2Fe_{14}B$, $Gd_2Fe_{14}B$, and $Nd_2Fe_{14}B$. The directions of the spin moments are parallel to c axis. The majority- (minority-) spin states are above (below) the zero axis.

To show the $3d$ states on the Fe sites in detail, spin-resolved partial DOS (PDOS) of $Y_2Fe_{14}B$, $Gd_2Fe_{14}B$, and $Nd_2Fe_{14}B$ are shown in Fig. 2. The left, middle, and right columns show the PDOS of $Y_2Fe_{14}B$, $Gd_2Fe_{14}B$, and $Nd_2Fe_{14}B$, respectively. Although different sites have different spin-resolved PDOS each other, the spin resolved PDOSs at same geometrical site in $Y_2Fe_{14}B$, $Gd_2Fe_{14}B$, and $Nd_2Fe_{14}B$ have similar features. One feature is complete saturation in the sense that the majority-spin band is almost fully occupied. The other is the Fermi energy always appears in a valley of the PDOS in the minority-spin band. These features are similar to the previous LSDA calculation.[15]

Spin-resolved PDOS on the R sites are shown in Fig. 3. The solid (dash) lines indicate f states (total) on the $R(f)$ and $R(g)$ sites. The occupied f states of $Nd_2Fe_{14}B$ are broad than that of $Gd_2Fe_{14}B$. There is difference of occupied f states between ferromagnetic and ferrimagnetic configuration. Total-energy difference between ferromagnetic and ferrimagnetic configurations of $4f$ and $3d$ spin sublattice is 2.17 eV. Ferrimagnetic configuration is more stable and this is in agreement with experimental results.

B. Magnetocrystalline anisotropy energy

Table I lists the calculated MAEs for $Y_2Fe_{14}B$, $Gd_2Fe_{14}B$, and $Nd_2Fe_{14}B$. The calculated values of MAE for $Y_2Fe_{14}B$ and $Gd_2Fe_{14}B$ are in agreement with the low-temperature-measured values, namely, 0.75 MJ/m^3 and 0.58 MJ/m^3, within 0.2 MJ/m^3 (i.e., 1.1 meV), respectively.[27] The values of the MAE for $Nd_2Fe_{14}B$ in ferromagnetic and ferrimagnetic configuration both are more than two times that of the MAE for $Y_2Fe_{14}B$ and $Gd_2Fe_{14}B$. The calculated MAEs of $Nd_2Fe_{14}B$ is compared with the value measured at room temperature, instead of with the value measured at low temperature. The calculated value of MAE of $Nd_2Fe_{14}B$ in ferrimagnetic configuration, i.e., 1.35 MJ/m^3 is less than the measured value, i.e., 4.27 MJ/m^3, at room temperature.[27]

Figure 4 shows the convergence of MAE of $Y_2Fe_{14}B$ and $Nd_2Fe_{14}B$ as a function of number of k sampling points. The convergence criterion was set to 10^{-6} hartree. The convergence of MAE of $Nd_2Fe_{14}B$ is achieved by using more than 500 k points. The convergence of MAE of $Y_2Fe_{14}B$ needs more than 1800 k points. The inclination of the convergence of $Y_2Fe_{14}B$ is more gradual than that of $Nd_2Fe_{14}B$. These results point out parallel sense of the relation between the convergence of MAE and the sampling k points with the result mentioned by Trygg *et al.*, namely, for $3d$ transition metals, 15 000 to 25 000 k points are needed to obtain MAE in the order of microelectron volts.[9] Thus, the material that has less MAE needs a greater number of k points to achieve convergence of MAE. For $R_2Fe_{14}B$, the calculation by using thousands of k points is therefore sufficient to obtain in the order of millielectron volts.

C. Magnetic moment and charge distribution

The magnetic moments of the Fe sites in $R_2Fe_{14}B$ had been investigated by several theoretical-research

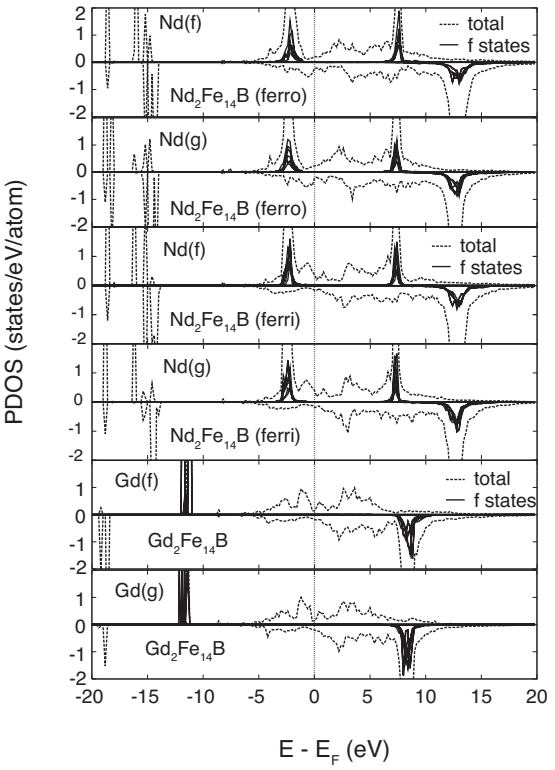

FIG. 3. Spin-resolved density of states on the rare-earth sites of $Nd_2Fe_{14}B$, and $Gd_2Fe_{14}B$. The directions of the spin moments are parallel to c axis. The majority- (minority-) spin states are above (below) the zero axis.

groups.[12,14,15] The results described below have similar tendency to previous self-consistent LSDA calculation results. Figure 5 compares our results on calculated local magnetic moment at the Fe sites of $Y_2Fe_{14}B$, $Gd_2Fe_{14}B$, and $Nd_2Fe_{14}B$ with previous experimental results obtained by neutron-diffraction and theoretical data for comparison.[15,28,29] The local magnetic moments at the different Fe sites in $Y_2Fe_{14}B$, $Gd_2Fe_{14}B$, and $Nd_2Fe_{14}B$ vary in the ranges of $2.34\mu_B-2.77\mu_B$, $2.35\mu_B-2.78\mu_B$, and $2.38\mu_B-2.78\mu_B$, respectively. The total local magnetic moments at the Fe sites are 34.81 μ_B/f.u., 35.09 μ_B/f.u., and 35.16 μ_B/f.u. for $Y_2Fe_{14}B$, $Gd_2Fe_{14}B$, and $Nd_2Fe_{14}B$, respectively. The $j2$ site has the largest moment, and the e site has the smallest moment for all the compounds. These tendencies of the local magnetic moment are in agreement with the neutron-

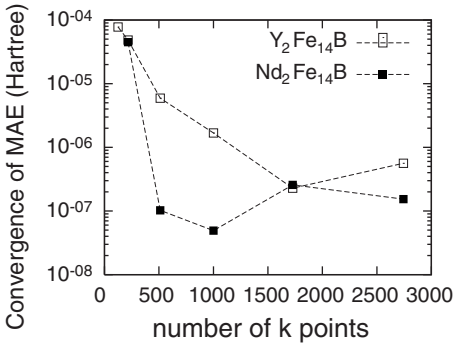

FIG. 4. Convergence of MAE for $Y_2Fe_{14}B$ and $Nd_2Fe_{14}B$.

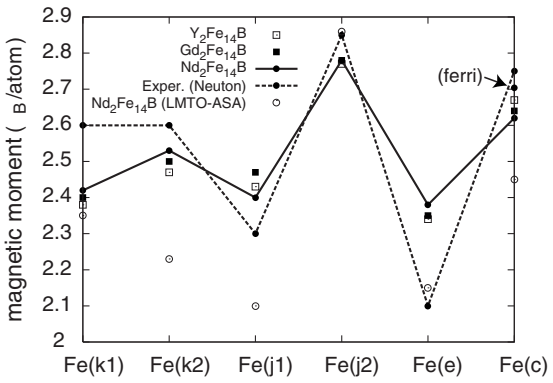

FIG. 5. Local magnetic moments of Fe sites in $Y_2Fe_{14}B$, $Gd_2Fe_{14}B$, and $Nd_2Fe_{14}B$. The ferri indicates the moment in ferrimagnetic configuration.

diffraction experiments mentioned above. The magnetic moments of the $k1$, $k2$, and e sites increase with substitution of Y(Gd) to Nd. On the contrary, the magnetic moments of the $j1$ and c sites decrease with substitution of Y(Gd) to Nd. These changes in the magnetic moments at the Fe sites show that the substitution of the R sites affects the magnetic moments on the Fe sites. Moreover, in $Nd_2Fe_{14}B$, there is no magnetic moment different between ferromagnetic and ferrimagnetic configurations of $4f$ and $3d$ spin sublattice, except Fe(c) sites.

Table II lists calculated magnetic moments of the $4f$ shells for $Gd_2Fe_{14}B$ and $Nd_2Fe_{14}B$. At both f and g sites of Gd, the spin moment is close to $7.0\mu_B$, and the orbital moments have vanished. These moments correspond well with the half-filled electron configuration of a Gd atom. On the other hand, at both f and g sites of Nd in ferromagnetic configuration, the spin moments are close to $3.8\mu_B$, and the orbital moments are $0.4\mu_B$, which are in disagreement with the magnetic moments of the Nd^{3+} ion. Moreover, the spin moments in ferrimagnetic configuration are increased to $4.6\mu_B$ but the orbital moments are still $0.4\mu_B$. Table I lists the calculated total magnetic moment. The lack of the orbital moment of Nd diminishes the total magnetic moment of $Nd_2Fe_{14}B$ in ferrimagnetic configuration.

The charge transfers of $Y_2Fe_{14}B$, $Gd_2Fe_{14}B$, and $Nd_2Fe_{14}B$ are listed in Table III. The variation in charge transfer with each site in $Nd_2Fe_{14}B$ has a similar tendency to that found in a previous work.[15] $Nd_2Fe_{14}B$ and $Gd_2Fe_{14}B$

TABLE II. Calculated magnetic moments of $4f$ shells for $R_2Fe_{14}B$ (R=Nd, Gd) (μ_B). Ferro (Ferri) indicates ferromagnetic (ferrimagnetic) configuration.

Configuration	Sites	Total	Spin	Orbital
Ferro	Nd(f)	3.41	3.82	−0.41
	Nd(g)	3.39	3.80	−0.41
Ferri	Nd(f)	−4.20	−4.61	0.41
	Nd(g)	−4.22	−4.64	0.41
Ferri	Gd(f)	−6.997	−6.994	−0.003
	Gd(g)	−7.018	−7.014	−0.004

TABLE III. Charge transfer for different sites in $R_2Fe_{14}B$ (R =Nd, Gd, Y) (unit is e).

			$Nd_2Fe_{14}B$	
Site	$Y_2Fe_{14}B$	$Gd_2Fe_{14}B$	Present	Ref. 15
$R(f)$	0.102	0.002	−0.146	−0.49
$R(g)$	0.067	−0.041	−0.162	−0.29
Fe($k1$)	0.075	0.049	0.105	0.03
Fe($k2$)	−0.013	0.001	0.020	0.01
Fe($j1$)	0.032	0.045	0.066	0.05
Fe($j2$)	−0.011	0.001	0.034	0.15
Fe(e)	0.158	0.076	0.178	−0.02
Fe(c)	0.039	0.060	0.083	0.11
B(g)	−0.656	−0.390	−0.656	0.02

both have the similar tendency regarding variation in charge transfer with each site. Moreover, there is really not much difference between ferrimagnetic and ferromagnetic configurations of $Nd_2Fe_{14}B$.

Density maps of the valence electron of $Gd_2Fe_{14}B$ and $Nd_2Fe_{14}B$ are shown in Fig. 6 and 7. In Fig. 6, the density maps at the (001) plane and (110) plane of $Gd_2Fe_{14}B$ are shown. The electron density of the Gd site is localized, and the low-density region (less than $0.02e/Å^3$) is expanded relatively more in the (001) plane. On the other hand, in the (110) plane, the low-density region near the Gd site is shrunk along the c axis. The electron-density maps in the figures described above are more of the results by the full-potential linearized augmented plane-wave (FLAPW) method[5] than that by the OLCAO method.[13] This implies that the self-consistent calculation using LCPAO method reproduces the charge distribution which obtained by the FLAPW method.

In Fig. 7, the density maps at the (001) and (110) planes of $Nd_2Fe_{14}B$ are shown. The shape of the low-density region is similar to the shape of that of $Gd_2Fe_{14}B$. As shown in Table III, there is no remarkable change in charge transfer between $Gd_2Fe_{14}B$ and $Nd_2Fe_{14}B$. Moreover, comparison of Fig. 6 and 7 reveals a difference in the charge densities at the Nd and Gd sites. The charge density at the Nd site has an aspherical shape but the charge density at the Gd site is spherical.

IV. DISCUSSION

As shown in Fig. 5, the magnetic moments of the Fe sites are in agreement with the reported neutron-diffraction experimental data. The magnetic moments of the Fe sites at same geometrical site in $Y_2Fe_{14}B$, $Gd_2Fe_{14}B$, and $Nd_2Fe_{14}B$ have similar trends. This geometrical site trend is corresponds to the PDOS of the Fe sites. The PDOS on the Fe sites and the value of the charge transfer of $Nd_2Fe_{14}B$ are similar to that of $Gd_2Fe_{14}B$ (see Fig. 2 and Table III). This suggests that the CEF of the contribution of the Fe sites of $Nd_2Fe_{14}B$ is similar to that of $Gd_2Fe_{14}B$.

Moreover, as shown in Fig. 6 and 7, no significant change is observed between the shapes of charge density at the interstitial region of $Gd_2Fe_{14}B$ and $Nd_2Fe_{14}B$. The low-density region of the charge distribution of $Nd_2Fe_{14}B$ in both ferromagnetic and ferrimagnetic configuration also have the same shape each other. These similarities of the charge distribution show that the charge distribution near the R atoms which is main contribution to CEF is not dramatically changed by the rare-earth element substitution.

The calculated MAEs are converged by using thousands of k points, and the MAEs of $Y_2Fe_{14}B$ and $Gd_2Fe_{14}B$ are in agreement with the measured values. Thus, as with another all electron calculation such as FLAPW, the LCPAO method is effective for the MAE calculations for intermetallics with no $4f$ electrons or half-filled $4f$ electrons.

Although, the correct configuration of $4f$ and $3d$ spin sublattice in $Nd_2Fe_{14}B$ is calculated, the calculated value of the MAE of ferrimagnetic configuration and the orbital moments of the $4f$ states are underestimated. In this work, the spherical averaged potential is used to describe the on-site Coulomb interaction within the rotationally invariant functional formation. This magnetic quantum number (m) independent of on-site potential causes less orbital polarization and the

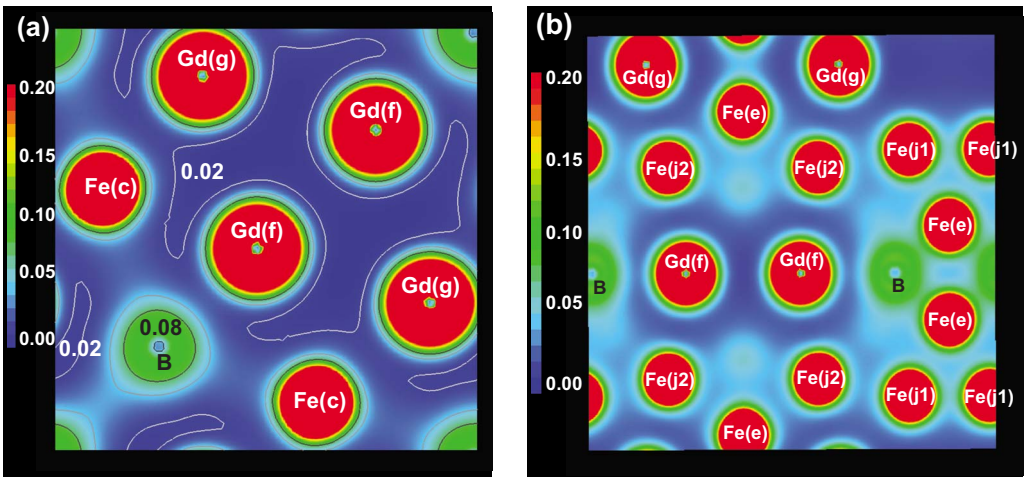

FIG. 6. (Color online) Valence-electron-density map of $Gd_2Fe_{14}B$ (a) map in (001) plane and (b) map in (110) plane. The unit of density is $e/Å^3$.

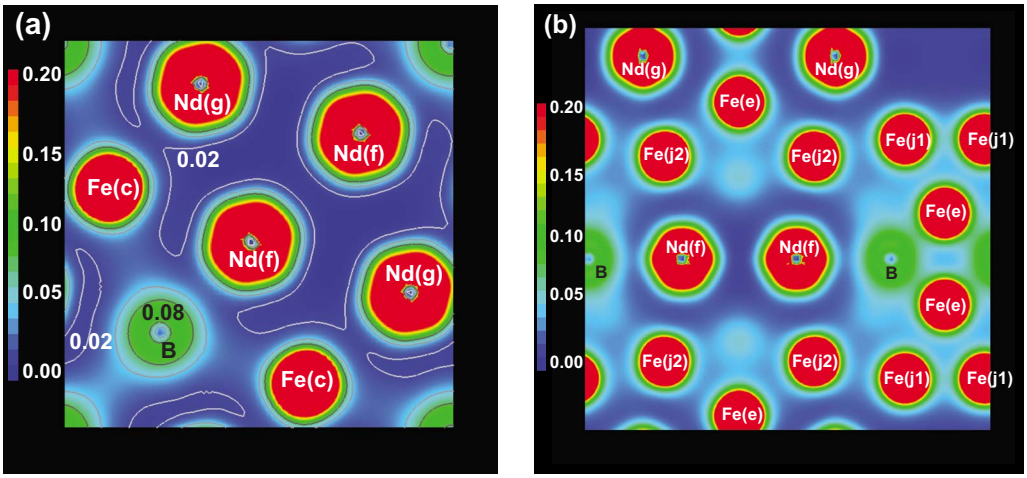

FIG. 7. (Color online) Valence-electron-density map of $Nd_2Fe_{14}B$ (a) map in (001) plane and (b) map in (110) plane. The unit of density is $e/Å^3$.

orbital moment. Thus, the *m*-dependent Coulomb interaction treatment in DFT+*U* formation brings in an improvement in the localized 4*f* states and the MAE.[30] Recently, Miletić and Blažina reported that improvement of the orbital moment on the Nd site of the $NdCo_5$ which were calculated by the *m*-dependent LDA+*U* formation with FLAPW method.[31]

V. SUMMARY

A relativistic DFT calculation using LCPAO with Hubbard-type on-site Coulomb potential *U* for *f* electrons in the *R* sites was performed. The calculated magnetic moments of $Y_2Fe_{14}B$ and $Gd_2Fe_{14}B$ are in agreement with the experimentally measured saturation moments of these compounds. The calculated MAEs of $Y_2Fe_{14}B$ and $Gd_2Fe_{14}B$ are also in agreement with the values experimentally measured at low temperature. Thus, the relativistic DFT calculation by using the LCPAO method is effective for *R* transition-metal intermetallics with closed or half-filled shells of 4*f* electrons. In addition, it was found that the charge density at the Nd sites has an aspherical shape that causes larger MAE of $Nd_2Fe_{14}B$ than that of $Gd_2Fe_{14}B$. However, the orbital moment of the open shell of 4*f* electrons at the Nd site and MAE were underestimated within the scope of a relativistic LDA+*U* with spherical average potential. The comparison of the electronic properties between $Gd_2Fe_{14}B$ and $Nd_2Fe_{14}B$ indicates that 4*f* electron treatment based on the orbital dependent on-site interaction is important for the improvement of the MAE calculation by using LCPAO method. Therefore, the relativistic DFT+*U* calculation by using the LCPAO method is effective for *R* transition-metal intermetallics when the *m*-dependent interactions of 4*f* states are recovered.

ACKNOWLEDGMENTS

The numerical calculations were carried out on the TSUBAME Grid Cluster at the Global Scientific Information and Computing Center of Tokyo Institute of Technology supported by the MEXT Open Advanced Research Facilities Initiative.

*isao.kitagawa.zd@hitachi.com

[1] E. Burzo and H. R. Kirchmayr, in *Handbook on the Physics and Chemistry of Rare Earth*, edited by K. A. Gchneidner and L. Eying (Elsevier Science, Amsterdam, 1989), Vol. 12, p. 71.
[2] X.-F. Zhong and W. Y. Ching, Phys. Rev. B **39**, 12018 (1989).
[3] Z. Zeng, Q. Q. Zheng, and W. Y. Lai, Phys. Rev. B **49**, 6741 (1994).
[4] L. Steinbeck, M. Richter, U. Nitzsche, and H. Eschrig, Phys. Rev. B **53**, 7111 (1996).
[5] M. Yamaguchi and S. Asano, Physica B **254**, 73 (1998).
[6] M. T. Hutchings, Solid State Phys. **16**, 227 (1964).
[7] H. Takayama, K.-P. Bohnen, and P. Fulde, Phys. Rev. B **14**, 2287 (1976).
[8] P. Bruno, Phys. Rev. B **39**, 865 (1989).
[9] J. Trygg, B. Johansson, O. Eriksson, and J. M. Wills, Phys. Rev. Lett. **75**, 2871 (1995).
[10] M. Kim, L. Zhong, and A. J. Freeman, Phys. Rev. B **57**, 5271 (1998).
[11] M. Colarieti-Tosti, T. Burkert, O. Eriksson, L. Nordström, and M. S. S. Brooks, Phys. Rev. B **72**, 094423 (2005).
[12] Z.-Q. Gu and W. Y. Ching, Phys. Rev. B **36**, 8530 (1987).
[13] W. Y. Ching and Z.-Q. Gu, J. Appl. Phys. **63**, 3716 (1988).
[14] S. S. Jaswal, Phys. Rev. B **41**, 9697 (1990).
[15] L. Nordström, B. Johansson, and M. S. S. Brooks, J. Phys.: Condens. Matter **5**, 7859 (1993).
[16] T. Ozaki, Phys. Rev. B **67**, 155108 (2003).
[17] T. Ozaki and H. Kino, Phys. Rev. B **69**, 195113 (2004).
[18] T. Ozaki and H. Kino, Phys. Rev. B **72**, 045121 (2005).
[19] M. J. Han, T. Ozaki, and J. Yu, Phys. Rev. B **73**, 045110 (2006).
[20] I. Kitagawa, J. Appl. Phys. **105**, 07E502 (2009).

[21] http://www.openmx-square.org/
[22] J. P. Perdew, K. Burke, and M. Ernzerhof, Phys. Rev. Lett. **77**, 3865 (1996).
[23] S. L. Dudarev, G. A. Botton, S. Y. Savrasov, C. J. Humphreys, and A. P. Sutton, Phys. Rev. B **57**, 1505 (1998).
[24] N. Singh, S. M. Saini, T. Nautiyal, and S. Auluck, J. Appl. Phys. **100**, 083525 (2006).
[25] A. B. Shick, A. I. Liechtenstein, and W. E. Pickett, Phys. Rev. B **60**, 10763 (1999).
[26] J. F. Herbst, J. J. Croat, F. E. Pinkerton, and W. B. Yelon, Phys. Rev. B **29**, 4176 (1984).
[27] S. Hirosawa, Y. Matsuura, H. Yamamoto, S. Fujita, and M. Sagawa, J. Appl. Phys. **59**, 873 (1986).
[28] D. Givord, H. S. Li, and F. Tasset, J. Appl. Phys. **57**, 4100 (1985).
[29] M. Sagawa, S. Fujimura, H. Yamamoto, Y. Matsuura, and S. Hirosawa, J. Appl. Phys. **57**, 4094 (1985).
[30] A. I. Liechtenstein, V. I. Anisimov, and J. Zaanen, Phys. Rev. B **52**, R5467 (1995).
[31] G. I. Miletić and Ž. Blažina, J. Magn. Magn. Mater. **321**, 3888 (2009).